NASA TECHNICAL MEMORANDUM

NASA TM X-72762

NASA TM X-72762

# REFLECTANCE CHARACTERISTICS OF THE VIKING LANDER CAMERA REFERENCE TEST CHARTS

By Stephen D. Wall, Ernest E. Burcher, and Daniel J. Jobson

(NASA-TM-X-72762) REFLECTANCE CHARACTERISTICS OF THE VIKING LANDER CAMERA REFERENCE TEST CHARTS (NASA) 31 p HC $3.75 CSCL 14E

N75-30511

Unclas G3/35 34290




NATIONAL AERONAUTICS AND SPACE ADMINISTRATION
LANGLEY RESEARCH CENTER, HAMPTON, VIRGINIA 23665

| 1. Report No. | 2. Government Accession No. | 3. Recipient's Catalog No. |
|---|---|---|
| NASA TM X-72762 | | |

| 4. Title and Subtitle | 5. Report Date |
|---|---|
| Reflectance Characteristics of the Viking Lander Camera Reference Test Charts | [illegible] |
| | 6. Performing Organization Code |
| 7. Author(s) Stephen D. Wall, Earnest E. Burcher, and Daniel J. Jobson | 8. Performing Organization Report No. |
| | 10. Work Unit No. |
| 9. Performing Organization Name and Address NASA Langley Research Center Hampton, VA 23665 | 11. Contract or Grant No. |
| | 13. Type of Report and Period Covered Technical Memorandum |
| 12. Sponsoring Agency Name and Address National Aeronautics & Space Administration Washington, DC 20546 | 14. Sponsoring Agency Code |

15. Supplementary Notes

16. Abstract

Reference test charts will provide radiometric, colorimetric, and spatial resolution references for the Viking lander cameras on Mars. Reflectance measurements of these references are described, including the absolute bidirectional reflectance of the radiometric references and the relative spectral reflectance of both radiometric and colorimetric references. Results show that the bidirection reflectance of the radiometric references is Lambertian to withing ±7% for incidence angles between 20° and 60°, and that their spectral reflectance is constant with wavelength to within ±5% over the spectral range of the cameras. Estimated accuracy of the measurements is ±0.04 in absolute reflectance, ±0.02 in relative bidirectional reflectance, and ±0.05 in relative spectral reflectance.

| 17. Key Words (Suggested by Author(s)) (STAR category underlined) | 18. Distribution Statement |
|---|---|
| Viking camera, calibration, optical scanner, Mars, reference test chart | Unclassified - Unlimited |

| 19. Security Classif. (of this report) | 20. Security Classif. (of this page) | 21. No. of Pages | 22. Price* |
|---|---|---|---|
| Unclassified | Unclassified | 28 | $5.75 |

*Available from { The National Technical Information Service, Springfield, Virginia 22151
STIF/NASA Scientific and Technical Information Facility, P.O. Box 33, College Park, MD 20740

# REFLECTANCE CHARACTERISTICS OF THE VIKING LANDER CAMERA REFERENCE TEST CHARTS

by

Stephen D. Wall, Ernest E. Burcher and Daniel J. Jobson

## SUMMARY

Reference test charts will provide radiometric, colorimetric, and spatial resolution references for the Viking lander cameras on Mars. Reflectance measurements of these references are described, including the absolute bidirectional reflectance of the radiometric references and the relative spectral reflectance of both radiometric and colorimetric references. Results show that the bidirectional reflectance of the radiometric references is Lambertian to within $\pm 7\%$ for incidence angles between 20° and 60°, and that their spectral reflectance is constant with wavelength to within $\pm 5\%$ over the spectral range of the cameras. Estimated accuracy of the measurements is $\pm 0.04$ in absolute reflectance, $\pm 0.02$ in relative bidirectional reflectance, and $\pm 0.05$ in relative spectral reflectance.

# INTRODUCTION

Each of the two Viking landers scheduled to land on Mars in 1976 will use two identical cameras to spatially, radiometrically, and (to a lesser extent) spectrally characterize the surrounding area. The camera is a multispectral radiometer with a mechanically scanning mirror, which provides the potential for high radiometric accuracy because of its use of single photodiodes to image an entire scene. The cameras feature an array of 12 silicon photodiodes, consisting of four broadband channels with selectable focus for high-resolution imaging, one broadband channel for rapid surveys, six narrowband channels for multispectral imaging (color and near-infrared), and one narrowband channel for scanning the sun. This capability requires that eleven calibrations be maintained for each camera throughout the life of the spacecrafts (since the sun-imaging diode is not calibrated). To help meet these calibration requirements each lander will carry three reference test charts (RTC). These charts provide eleven reflectance references (grey scales) for radiometric calibration of the cameras, three colorimetric references for reconstruction of color images, and three sets of tribar patterns for testing spatial frequency response.

Of primary importance are the reflectance characteristics of the grey scales, which are used for absolute radiometric calibration. This paper presents measurements of their absolute bidirectional reflectance and relative spectral reflectance, which together provide the required reflectance data. This paper also presents measurements of the relative spectral reflectance of the color patches, spatial data about the tribars, and an error analysis of the reflectance measurements.

## LIST OF SYMBOLS

| | |
|---|---|
| $g$ | phase angle, deg |
| $H(\lambda)$ | gonioradiometer sample plane illumination, $W/cm^2-\mu m$ |
| $I$ | photosensor signal current, A |
| $I_n$ | photosensor noise current, A |
| $k$ | number of encoding levels |
| $r(\iota, \varepsilon, g, \lambda)$ | absolute spectral bidirectional reflectance |
| $r_h$ | $MgCO_3$ (reference) broadband hemispherical reflectance |
| $r_i(\iota, \varepsilon, g)$ | broadband bidirectional reflectance |
| $r_r(\iota, \varepsilon, g)$ | $MgCO_3$ (reference) broadband bidirectional reflectance |
| $R_i(\iota, \varepsilon, g)$ | equivalent Lambertian reflectance |
| $R(\lambda)$ | responsivity, A/W |
| $V_d$ | drift, V |
| $V_n$ | photosensor rms noise, V |
| $V_q$ | quantization noise, V |
| $V$ | dynamic range, V |
| $\delta_i(\iota, \varepsilon, g)$ | reflectance deviation from Lambertian |
| $\Delta_i$ | largest reflectance deviation from Lambertian over all measured incidence angles, $10° \leq \iota \leq 80°$ |
| $\Delta'_i$ | largest reflectance deviation from Lambertian over restricted range of incidence angles, $20° \leq \iota \leq 60°$ |
| $\varepsilon$ | viewing angle, deg |
| $\iota$ | illumination angle, deg |
| $\lambda$ | wavelength, $\mu m$ |

| | |
|---|---|
| $\phi(\iota, \varepsilon, g)$ | illumination scattering function |
| $\rho(\lambda)$ | spectral reflectance |
| $\rho_r^j(\lambda)$, j=1,2,...5 | published measurements of $MgCO_3$, reflectance |
| $\tau_\ell(\lambda)$ | Viking camera lens transmission |

Subscripts

| | |
|---|---|
| i | i'th RTC grey patch |
| r | $MgCO_3$ reference |

Superscripts

| | |
|---|---|
| * | absolute measurement |
| ~ | relative measurement (normalized to 1.0) |
| — | average |

## GENERAL DESCRIPTION

## OF THE REFERENCE TEST CHART

### Physical Characteristics

The reference test chart, shown in figure 1, consists of eleven 2.5 cm square grey patches, three 2.5 cm square red, green and blue patches, and three sets of tribar patterns. The tribars, which are used to evaluate the cameras spatial frequency response, consist of grey material having a reflectance of 0.40 and black bars having a reflectance of 0.02 (ref. 1). The spatial frequencies of the tribar patterns were measured on six non-flight test charts. Average spatial frequencies and deviations from the average for the six measured charts are summarized in Table I. The two white patches in the upper left and right corners contain boron nitride and antimony oxide pigments, which change reflectance with the amount of absorbed ultraviolet light. These patches are intended to measure ultraviolet light levels on Mars as a part of the Viking Physical Properties Science Team experiments.

### Location

Three test charts are mounted on each of the two Viking landers as shown in figure 2. Each camera has its own chart located 1.0 m from it with the chart surface normal to the camera line of sight. The third chart is 1.11 m from each camera, oriented normal to the plane containing both camera lines of sight and forming a 23° angle with each.

The charts are located on the top of the lander between the two radio-isotope-thermoelectric generators. This location protects the test charts to

some extent from degradation by windblown sand. However, it also permits reflection from parts of the lander structure to add to the light incident on the charts, which impairs the accuracy of radiometric calibration. Another disadvantage of the charts locations is that their remoteness from the Mars surface complicates comparisons with the Martian surface. Special imaging sequences are required to view the reference test charts, and different illumination and viewing geometries must be accounted for.

## Use For Radiometric Calibration

The primary purpose of the test chart is to provide reference surfaces with known reflectance properties which can be compared to elements of the Martian surface to determine their reflectance without relying on pre-flight calibrations. It makes such comparisons appreciably easier if the reference surfaces have a spectrally flat reflectance within the camera spectral bandwidth and a Lambertian illumination scattering function (ref. 2). High accuracy calibration using the test charts would require that any departures of the reflectances from spectral flatness or Lambertian scattering be taken into consideration before making comparisons with the Mars surface.

## MEASUREMENT THEORY AND PROCEDURES

### Assumptions and Theory

Separation of variables.- Complete characterization of absolute reflectance $r^*(\iota, \varepsilon, g, \lambda)$ as a function of wavelength and illumination and viewing geometry is generally not practical because of the large number of measurements involved. It has therefore become customary to assume that the wavelength dependence of the reflectance function is independent of illumination and viewing angles, and hence to separate absolute spectral reflectance or albedo, $\rho^*(\lambda)$, from relative bidirectional reflectance or illumination scattering function, $\tilde{\phi}(\iota, \varepsilon, g)$, so that

$$r^*(\iota, \varepsilon, g, \lambda) = \rho^*(\lambda) \quad \tilde{\phi}(\iota, \varepsilon, g)$$

where $\iota$ is the illumination angle, $\varepsilon$ the viewing angle, $g$ the phase angle, and $\lambda$ wavelength. The tilde ($\tilde{}$) is used to indicate normalization to a peak value of 1.0, and the asterisk (*) to indicate an absolute measurement.

The use of this separation in measuring $r^*(\iota, \varepsilon, g, \lambda)$ has the inherent disadvantage that it requires narrowband absolute measurements. If instead the absolute bidirectional reflectance is measured with a spectrally unfiltered (i.e., broadband) photosensor, then higher signal-to-noise ratios, and hence accuracies, can be obtained for the wide bandwidth required to make rapid measurements. For this reason, the absolute reflectance of the $i$'th test chart patch, $r_i^*(\iota, \varepsilon, g, \lambda)$ is assumed to be separable into

$$r_i^*(\iota, \varepsilon, g, \lambda) = \tilde{\rho}_i(\lambda)\, r_i^*(\iota, \varepsilon, g) \qquad (1)$$

where $\tilde{\rho}_i(\lambda)$ is the relative spectral reflectance, $0 \leq \tilde{\rho}_i \leq 1.0$, and $r_i^*(\iota,\varepsilon, g)$ the absolute bidirectional reflectance.

Absolute bidirectional measurements.- The absolute bidirectional reflectance of the grey patches was determined by measuring the radiance of the i'th RTC patch relative to that of a magnesium carbonate ($MgCO_3$) reference under identical illumination. The ratio of signals generated by these radiances is given by

$$\frac{I_i(\iota, \varepsilon, g)}{I_r(\iota=10^\circ, \varepsilon=0^\circ, g=10^\circ)} = \frac{r_i^*(\iota, \varepsilon, g) \int H(\lambda)\, \rho_i(\lambda)\, R(\lambda)\, \tau_\ell(\lambda)\, d\lambda}{r_r^*(\iota=10^\circ, \varepsilon=0^\circ, g=10^\circ) \int H(\lambda)\rho_r(\lambda)R(\lambda)\tau_\ell(\lambda)\, d\lambda}$$

where $I$ is the detector signal and $H(\lambda)$ the irradiance of the sample plane. A comparison with magnesium carbonate was made at $\iota = 10^\circ$, $\varepsilon = 0^\circ$, $g = 10^\circ$ to avoid the known backscatter peak near zero phase angle yet maintain high signal level. For this geometry, the value of $r_r$ is taken to be $(0.968)(\cos 10^\circ)$, which is a mean value of published data as discussed later in the error analysis section. The cosine factor can be used because the magnesium carbonate is a nearly Lambertian scatterer for the selected illumination and viewing geometry (ref. 3). If it is also assumed that the grey scales and reference are spectrally similar, so that

$$\int H(\lambda)\rho_i(\lambda)R(\lambda)\tau_\ell(\lambda)d\lambda \approx \int H(\lambda)\rho_r(\lambda)R(\lambda)\tau_\ell(\lambda)d\lambda$$

then the following equation results for the absolute bidirectional reflectance of the i'th RTC grey patch:

$$r_i^*(\iota, \varepsilon, g) = \frac{I_i}{I_r}(0.968)(\cos 10^\circ) \qquad (2)$$

The equivalent geometric Lambertian reflectance, $R_i$, is given by

$$R_i(\iota, \varepsilon, g) = r'_i(\iota, \varepsilon, g)/\cos \iota \qquad (3)$$

It is convenient to express the deviation from Lambertian reflectance at each point as

$$\delta_i(\iota, \varepsilon, g) = |R_i(\iota, \varepsilon, g) - \overline{R}| \qquad (4)$$

where $\overline{R}$ is the average of the $R_i$ over all measured illumination angles. The largest of these, $\Delta_i$, is reported here as an overall measure of deviation from Lambertian. A somewhat more useful measure is $\Delta'_i$, the maximum deviation of each patch from Lambertian over the more limited range of illumination angles $20° \leq |\iota| \leq 60°$ likely to be useful for imaging on Mars. In this range, deviations from Lambertian are much smaller.

## Instrumentation

Absolute Bidirectional Measurements.- A bidirectional gonioradiometer was developed which could make rapid, computer-assisted measurements on the reference test charts. The gonioradiometer is shown in figure 3. Both the illumination and viewing arms are gimbal mounted on two axes to provide movement in azimuth and elevation directions and are positive indexed at 5° intervals to ensure accurate positioning.

A tungsten filament lamp mounted 41 cm from the sample acts as source for the illumination. The filament subtends a 0.4° angle from the sample plane. Baffling limits the area illuminated to an area 5 cm in diameter, also limiting the stray light reflected to the sample from the gimbals of

the gonioradiometer. The area illuminated in the sample plane is uniform to within less than 1% in the viewing area, as shown in figure 4. The irradiance in the sample plane is 140$\mu W/cm^2$ in the silicon bandwidth. The sample plane contains a movable slide holding the test chart, a block of magnesium carbonate, and a Rayleight terminator, which serves as a dark reference. A Rayleigh terminator is a glass horn, painted black on the outside, which reflects light incident on the opening towards the inside and thus absorbs essentially all of the incident light (ref. 4).

The viewing head is composed of a silicon detector similar to the broad-band Viking camera detectors, and a Viking camera lens, mounted so that the second principal plane of the lens is 48 cm from the sample plane. The detector field of view at the sample plane is roughly circular with a diameter of 0.2 cm. The detector sensitivity profile is shown in its correct relation to the illuminated area in figure 4.

Signals from the detector were amplified and processed through a 24 Hz electronic filter. This bandwidth was chosen as a compromise between reducing electronic noise and making measurements rapidly. A 12-bit analog to digital conversion was performed with a time aperture of 20 $\mu s$, and the resulting digital word was fed to an HP 2100A computer for data reduction and plotting.

The measurement procedure was as follows. First, the magnesium carbonate block was placed in the sample area and the resulting signal stored in the computer. The Rayleigh terminator was then substituted and the signal stored as a zero reflectance (dark current) signal. The patch to be measured was then placed in the sample plane and the photosensor signal was recorded for illumination angle settings from -90° to +90° in the azimuth direction in 10° increments, and from -15° to +90° in the elevation direction, in 15° increments.

The position $i = e = 0°$ was skipped since the illumination and viewing optics could not occupy the same space. This range of elevation and azimuth illumination angles covers the anticipated range of sun incidence angles on the test chart on Mars.

Relative Spectral Measurements.- The relative spectral reflectance of the test chart patches was measured using a Cary model 14 recording spectrophotometer with a model 1411 diffuse reflectance attachment. The total spectral range of the measurement was 0.35 to 1.10 μm, with spectral resolution of 0.0001 μm.

Measurements were made from 0.4 to 0.65 μm by alternately illuminating an area 2.2 cm by 0.79 cm of each test chart patch and a magnesium carbonate reference with monochromatic light at 5° incidence angle. An integrating sphere collected the light from sample or reference, and the sphere output was measured by a 1P28 phototube. From 0.65 to 1.10 μm the instrument requires that the path be reversed. White light diffusely illuminated the sample and reference through the integrating sphere, and sample and reference were alternately viewed at 5° by a monochromator and lead sulfide detector (ref. 5). In this mode there was considerably more system noise, as is accounted for by the error analysis.

## RESULTS

Absolute bidirectional reflectance measurements.- From the bidirectional reflectance data, graphs of reflectance versus azimuth illumination angle were prepared at each elevation angle. From these graphs, the average equivalent Lambertian reflectance was determined as discussed earlier (see equation 4). The maximum deviation from Lambertian over the full measurement range and over the reduced range $20° \leq \iota \leq 60°$, $\Delta_i$ and $\Delta_i'$, were calculated. These data are shown in Table II for the three measured charts, identified by their serial numbers 14, 15 and 17. The mean of these three, together with maximum deviation from this mean, is also shown. These data may be used as an estimate of the reflectance of the other three test charts. It may be noted that in all cases the maximum deviation from Lambertian over the full range of illumination is less than $\pm$11 percent and over the reduced range is less than $\pm$7.5 percent. Target-to-target variations are less than $\pm$2.5 percent.

Relative spectral reflectance measurements.- Spectral measurements made on a non-flight RTC (serial number 2) are shown in figure 5(a). These measurements are relative to magnesium carbonate, and absolute levels vary from chart to chart as discussed above. Spectral curves for the color patches are shown in figure 5(b).

The data shows that the grey patches are spectrally flat to within $\pm$0.02 reflectance unit, which is within the experimental error. The reflectance curves of the grey patches tend to rise slightly towards shorter wavelengths, which may be a result of the lower blue reflectance of the reference (figure 6). Four of the grey patches also show a noticeable increase in the infrared. The three color patches have very high infrared reflectance, the green and blue

patches showing an abrupt change around 0.7 μm. Since the eye is not sensitive to radiation past 0.7 μm, this contribution should not affect visual color. But because of infrared leaks in the camera color filters and the silicon diode increased sensitivity in the 0.7 to 0.9 μm region, this high infrared reflectance will tend to reduce the accuracy to which these colors will be reconstructed (ref. 6 and 9).

## ERROR ANALYSIS

Errors introduced by assumptions made to simplify measurements, by the measurements themselves, and by the calibration standard must be accounted for to determine the error budget of the reflectance measurements. In general, the error sources are not strongly dependent on the magnitude of the signal. Thus it is appropriate to present errors as absolute rather than percentage, since these errors represent increasingly larger percentages towards the lower reflectances.

Shot and Johnson noise, drift, non-repeatability errors, instrumentation and reference standard errors are assumed to be statistically independent. Quantization noise is not strictly independent of drift as it is of the other noise sources, but the error introduced by treating it as independent is negligible.

### Simplifying Assumptions

In a preceding section, the assumption was made that

$$\frac{\int H(\lambda)\rho_r^*(\lambda)\tau_\ell(\lambda)R(\lambda)\,d\lambda}{\int H(\lambda\ \rho_i^*(\lambda)\tau_\ell(\lambda)R(\lambda)\,d\lambda} \approx 1$$

The error in the assumption can be estimated by a numerical integration of both integrals. Using National Bureau of Standards irradiance measurements for $H(\lambda)$, magnesium carbonate reflectance data from reference 5 for $\rho_r^*(\lambda)$ and measured values for the lens transmittance $\tau_\ell(\lambda)$ and photosensor

responsivity $R(\lambda)$, the maximum value of the ratio was found to be 1.016. The assumption, and therefore this error, applies only to the bidirectional measurements.

## Measurement Errors

Bidirectional reflectance measurements.- Angular positioning errors of source and detector, sample and reference position errors, and non-coincidence of the gonioradiometer axes are negligible because of the large dimensions and accurate construction of the gonioradiometer.

Silicon detectors are known to have drift in dark current levels. To eliminate the effect of this drift both dark and reference measurements were made at each elevation illumination angle setting. Thus at most 5 to 10 seconds elapsed between data points and dark or reference points. Typical voltage drift during this time period, $V_d$, was observed to be less than 2 mV.

The error sources in the signal processing chain are (1) shot noise resulting from the random passage of carriers across the photodiode junction; (2) Johnson noise generated by the preamplifier load resistor; and (3) quantization noise which occurs as a result of the limited accuracy of the analog-to-digital converter.

The shot noise current is determined by the photodiode current (ref. 8) and is approximately $2 \times 10^{-15}$ $A/\sqrt{Hz}$ for this circuit. Johnson noise is a function of preamplifier load resistance and is approximately $2 \times 10^{-14}$ $A/\sqrt{Hz}$. The total electronic noise current is thus

$$I_n = \sqrt{24} \quad (2^2 + 0.2^2)^{1/2} \times 10^{-14} \approx 10^{-13} \text{ amp}$$

and the noise voltage is

$$V_n = (10^8\ \Omega)(10^{-13}\ A) = 10^{-5}\ V$$

The peak-to-peak voltage excursion is about four times this value or approximately 40 μV.

Quantization noise, $V_q$, is given by (ref. 7)

$$V_q = \frac{\Delta V^2}{12k^2} = 5.4 \times 10^{-3}\ V$$

where $\Delta V(=10V)$ is the total dynamic range and $k(=64)$ is the number of quantization levels.

The total noise voltage is thus

$$(V_d^2 + (4V_n)^2 + V_q^2)^{1/2} = 6\ mV$$

A 10 volt signal represents a reflectance of 1.00. Therefore the total noise represents an error of 0.0006 in reflectance.

As a further test of error on the gonioradiometer, dual runs were made of several patches at one elevation angle. The results show that maximum repeatability error occured where signal levels were lowest, at high illumination angles. The largest lack of repeatability was 0.02 reflectance units. The source of the discrepancy between the relatively large repeatability errors compared to the small predicted system noise was not investigated. Rather, an overall possible error of 0.02 was assumed for the measurements even though errors of this magnitude were observed only at low illumination angles.

Relative spectral measurements.- Reference 5 contains a detailed description of the Cary 14 recording spectrophotometer, together with an extensive error analysis which yields the following results:

| | |
|---|---|
| Instrumentation errors | 0.01 |
| Integrating sphere inefficiency | 0.01 |
| Standard material reflectance error | 0.04 |

The total error is thus 0.042. System noise, not included in the referenced analysis, amounts to 0.0005 in reflectance for the visible (0.4 to 0.65 μm) and 0.002 for the infrared (0.65 to 1.10 μm). Taking the worse of these as an upper bound, total errors combine to 0.047.

## Errors in Calibration Standard

A single magnesium carbonate block, viewed at 10° illumination angle, was used as a standard reference in the absolute reflectance measurements. A similar block was used as the diffuse reflectance reference for the relative spectral measurements. In the bidirectional measurements, a 10° illumination angle eliminated the errors associated with the backscatter peak which exists near zero phase angle. However, the calibration accuracy of the blocks is subject to error, an error which applies to both relative spectral and absolute reflectance measurements.

Reference 5 presents five independent assessments of the hemispherical reflectivity of $MgCO_3$, here referred to as $\rho_r^{(j)}$, $j = 1, 2, \ldots 5$ and reproduced in figure 6. The value used in this paper was obtained by averaging these measurements at small wavelength intervals and numerically integrating over the cameras spectral bandwidth using normalized silicon responsivity as the weighting factor; that is,

$$\bar{R}_r = \frac{\int \bar{\rho}(\lambda)\, R(\lambda)\, d\lambda}{\int R(\lambda)\, d\lambda}$$

where

$$\bar{\rho}(\lambda) = \frac{1}{5} \sum_{j=1}^{5} \rho_r^{(j)}(\lambda)$$

The resulting value is

$$\bar{R}_r = 0.968 \pm 0.025$$

The error value results from taking highest and lowest reflectance data given.

In addition, $MgCO_3$ may have a reflectance slightly less than a Lambertian scatterer at 10° illumination. Data from reference 3 indicate that the illumination scattering function is less than 0.02 below Lambertian at this angle. Therefore, the total calibration error is estimated as the root-sum-square of these, 0.032.

## Total Error

The error sources discussed above, with the exception of the random photosensor and preamplifier noise which is negligible, are summarized below:

| Measurement | Error | |
|---|---|---|
| Absolute bidirectional reflectance | absolute | relative |
| repeatability | ±0.02 | ±0.02 |
| calibration standard | 0.032 | - |
| theory assumption | 0.016 | - |
| root-sum-square | ±0.041 | ±0.02 |

| Measurement | Error | |
|---|---|---|
| Relative spectral reflectance | absolute | relative |
| noise | | ±0.02 |
| system (from ref. 3) | | 0.042 |
| root-sum-square | | ±0.047 |

## CONCLUSION

Broadband bidirectional reflectance characteristics of three of the six Viking lander camera reference test charts and spectral reflectance of one non-flight test chart have been measured. Equivalent Lambertian reflectance and maximum deviation from Lambertian are presented for the eleven grey patches on each chart. Spectral curves for grey and color patches of the non-flight chart are also presented.

Bidirectional reflectance measurements of the grey patches show them to be Lambertian to within $\pm 11$ percent for incidence angles from 10° to 80°, and within $\pm 7$ percent for incidence angles from 20° to 60°. Variations between the measured flight charts is less than $\pm 3$ percent. Spectral measurements indicate that the grey patches are spectrally flat to within $\pm 5$ percent, with a general tendency toward higher reflectance in the near infrared. The three color patches are narrowband in the visual color region from 0.4 to 0.7 μm, but they have very high reflectance beyond 0.7 μm, which complicates their use as colorimetric standards because of infrared leaks in the cameras response.

Estimated errors are $\pm 0.04$ in absolute reflectance; $\pm 0.02$ in relative illumination scattering function; and $\pm 0.05$ in relative spectral reflectance.

## REFERENCES


1. Anon: Reference Test Chart. PD837D 3500200, Martin-Marietta Corporation.

2. Jobson, Daniel J.: Paint Surface Reflectance Properties Related to a Calibration Target for the Viking Lander Imaging System. NASA LWP-976, 1971.

3. Janssen, J. E.; and Toborg, R. H.: Measurement of Spectral Reflectance Using an Integrating Hemisphere. NASA SP-31, 1963, pp. 169-181.

4. Ditchburn, R. W.: Light. Interscience Publishers, 1963, p. 586.

5. Gaumer, R. E.; Streed, E. R.; and Vajta, T. F.: Methods for Experimental Determination of the Extra-Terrestrial Solar Absorptance of Spacecraft Materials. NASA SP-31, 1963, pp. 135-146.

5A. Dunkle, R. V.: Spectral Reflectance Measurements. First Symposium on Surface Effects in Spacecraft Materials, (F. J. Clauss, ed.), John Wiley and Sons, Inc., 1960, p. 117. (Primary reference is reference 5)

5B. Betz, H. T.; Olson, O. H.; Schurin, B. D.; and Morris, J. C.: WADC Tech. Rep. 56-222, Armour Research Foundation, May 1957. (Primary reference is reference 5.)

6. Huck, F. O.; et. al: The Viking Mars Lander Camera. In preparation.

7. Carlson, A. Bruce: Communications Systems. McGraw-Hill Book Company, C. 1968.

8. Kelly, W. Lane, IV; and Katzberg, Stephen J.: Investigation of Responsivity and Noise in a Direct-Coupled Photodetector-Preamplifier for Facsimile Camera. NASA TN D-7338, 1973.

9. Mutch, T. A.; et. al.: Viking Imaging Science Test Report (private communication)

TABLE I

Spatial Frequencies of Tribar Patterns

| Pattern Location | Average Spatial Frequency*, lp/mm | Maximum Deviation, lp/mm |
|---|---|---|
| Top | 0.078 | ±.001<br>-.006 |
| Center | 0.154 | +.004<br>-.001 |
| Bottom | 0.225 | +.003<br>-.003 |

*Average of six non-flight charts

TABLE II: GREY SCALE REFLECTANCE

| RTC | | Patch No. | | | | | | | | | | |
|---|---|---|---|---|---|---|---|---|---|---|---|---|
| 14 | $R_n$ | 0.095 | 0.127 | 0.191 | 0.242 | 0.302 | 0.355 | 0.400 | 0.448 | 0.529 | 0.566 | 0.751 |
| | $\Delta_n(10° \leq i \leq 80°)$ | 0.010 | 0.006 | 0.006 | 0.007 | 0.013 | 0.010 | 0.009 | 0.011 | 0.020 | 0.015 | 0.033 |
| | $\Delta'_n(20° \leq i \leq 60°)$ | .006 | 0.005 | 0.005 | 0.007 | 0.013 | 0.010 | 0.006 | 0.011 | 0.007 | 0.007 | 0.023 |
| 15 | $R_n$ | 0.095 | 0.133 | 0.202 | 0.253 | 0.305 | 0.361 | 0.403 | 0.461 | 0.530 | 0.574 | 0.770 |
| | $\Delta_n(10° \leq i \leq 80°)$ | 0.014 | 0.014 | 0.012 | 0.013 | 0.031 | 0.017 | 0.018 | 0.015 | 0.029 | 0.021 | 0.043 |
| | $\Delta'_n(20° \leq i \leq 60°)$ | 0.006 | 0.006 | 0.006 | 0.008 | 0.009 | 0.010 | 0.012 | 0.010 | 0.013 | 0.011 | 0.027 |
| 17 | $R_n$ | 0.095 | 0.129 | 0.196 | 0.241 | 0.318 | 0.351 | 0.395 | 0.464 | 0.521 | 0.577 | 0.765 |
| | $\Delta_n(10° \leq i \leq 80°)$ | 0.008 | 0.008 | 0.011 | 0.013 | 0.020 | 0.013 | 0.014 | 0.015 | 0.025 | 0.016 | 0.042 |
| | $\Delta'_n(20° \leq i \leq 60°)$ | 0.006 | 0.006 | 0.007 | 0.009 | 0.009 | 0.013 | 0.007 | 0.010 | 0.012 | 0.013 | 0.032 |
| Average | | 0.095 | 0.130 | 0.196 | 0.245 | 0.308 | 0.356 | 0.399 | 0.458 | 0.527 | 0.572 | 0.762 |
| Max. Deviation | | 0 | +0.003 | +0.006 | +0.004 | +0.100 | -0.005 | +0.004 | -0.010 | -0.006 | -0.006 | -0.011 |

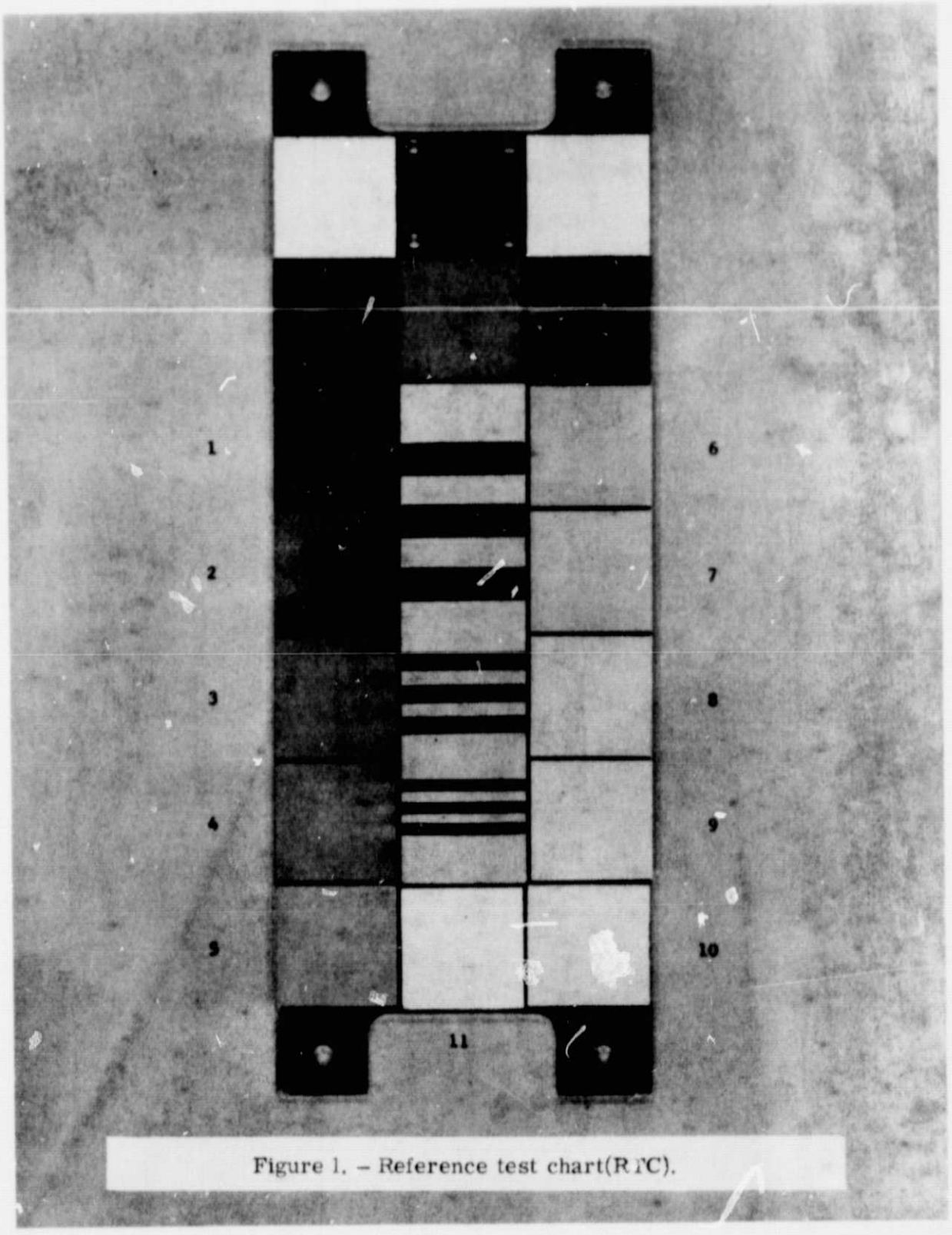


Figure 1. – Reference test chart(RTC).

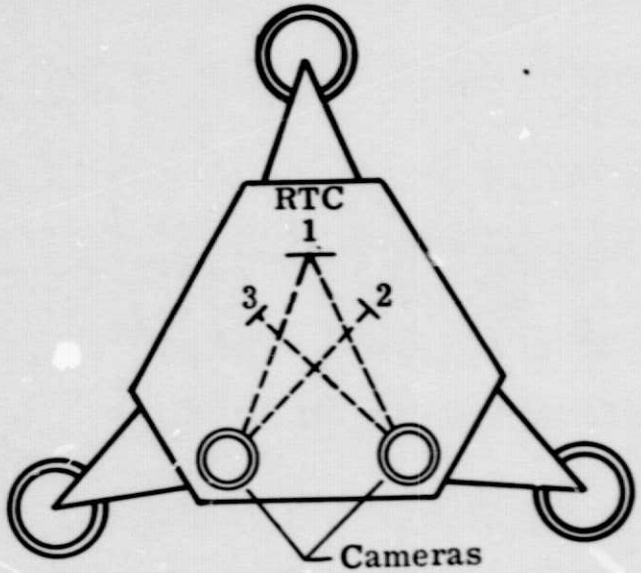


Figure 2.- RTC location on lander.

Figure 3.- Bidirectional gonioradiometer.

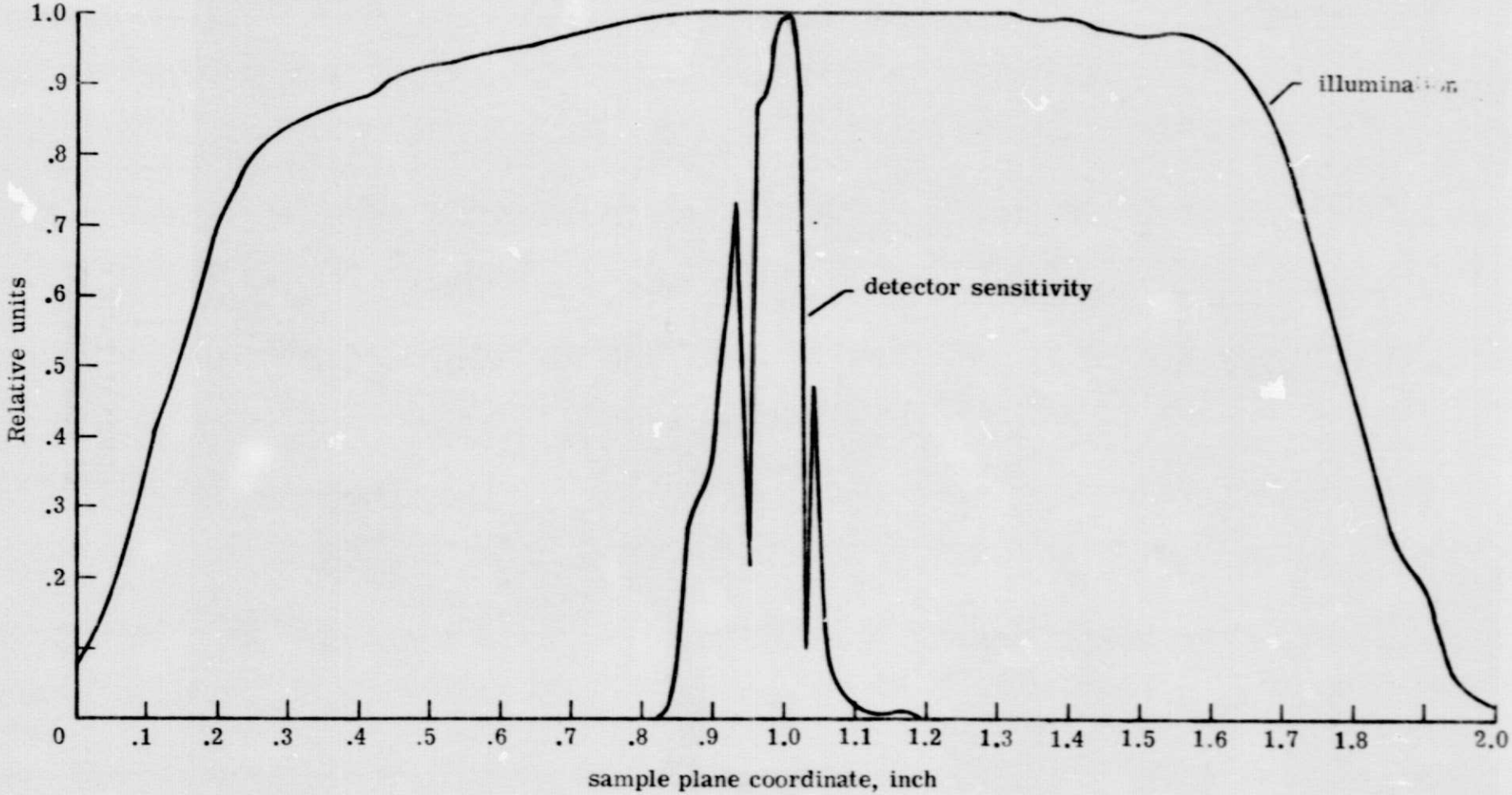


Figure 4.– Relative illumination and detector sensitivity in the gonioradiometer sample plane.

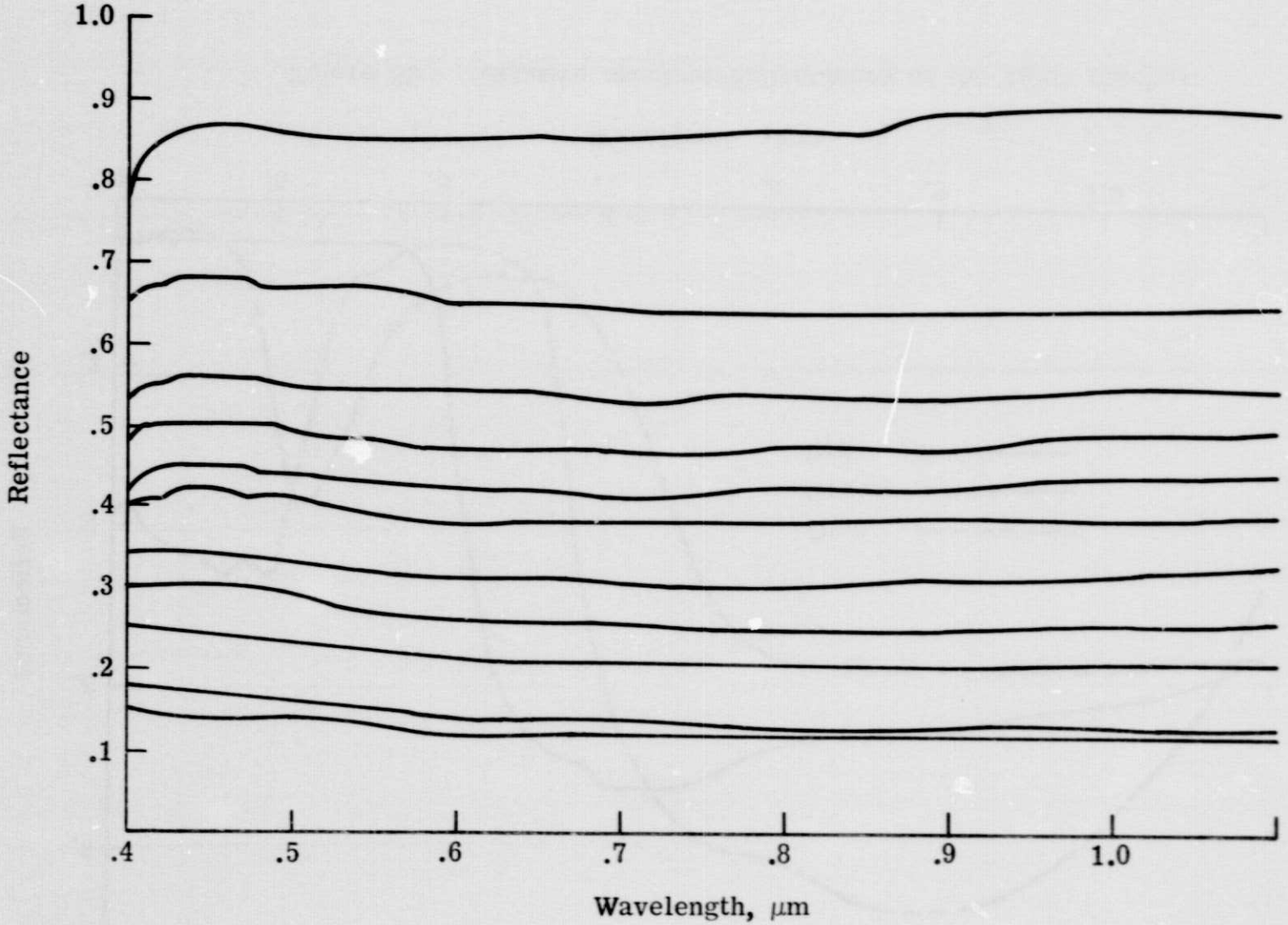


Figure 5a.- Relative spectral reflectances of gray patches

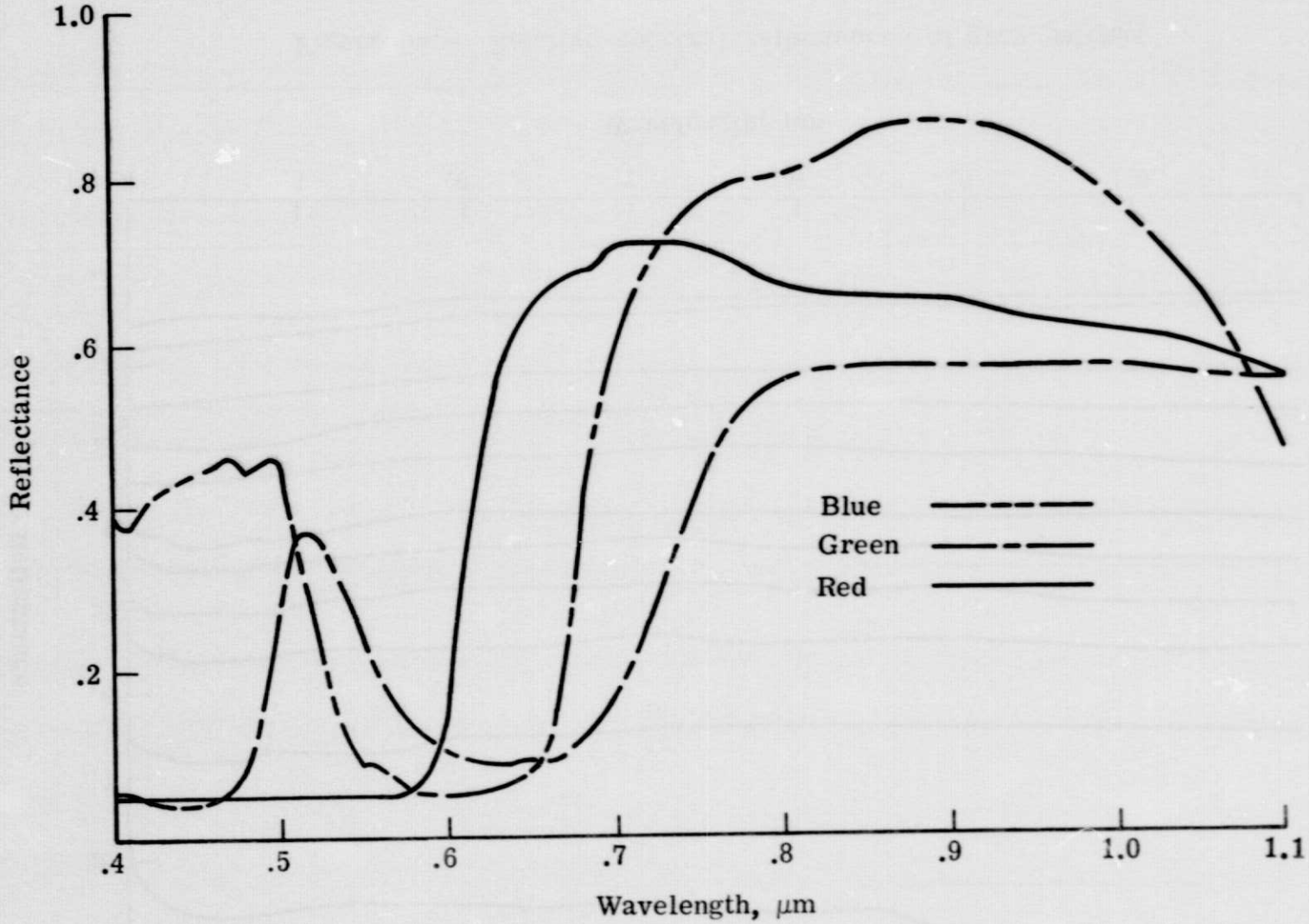


Figure 5b.- Relative spectral reflectances of the color patches.

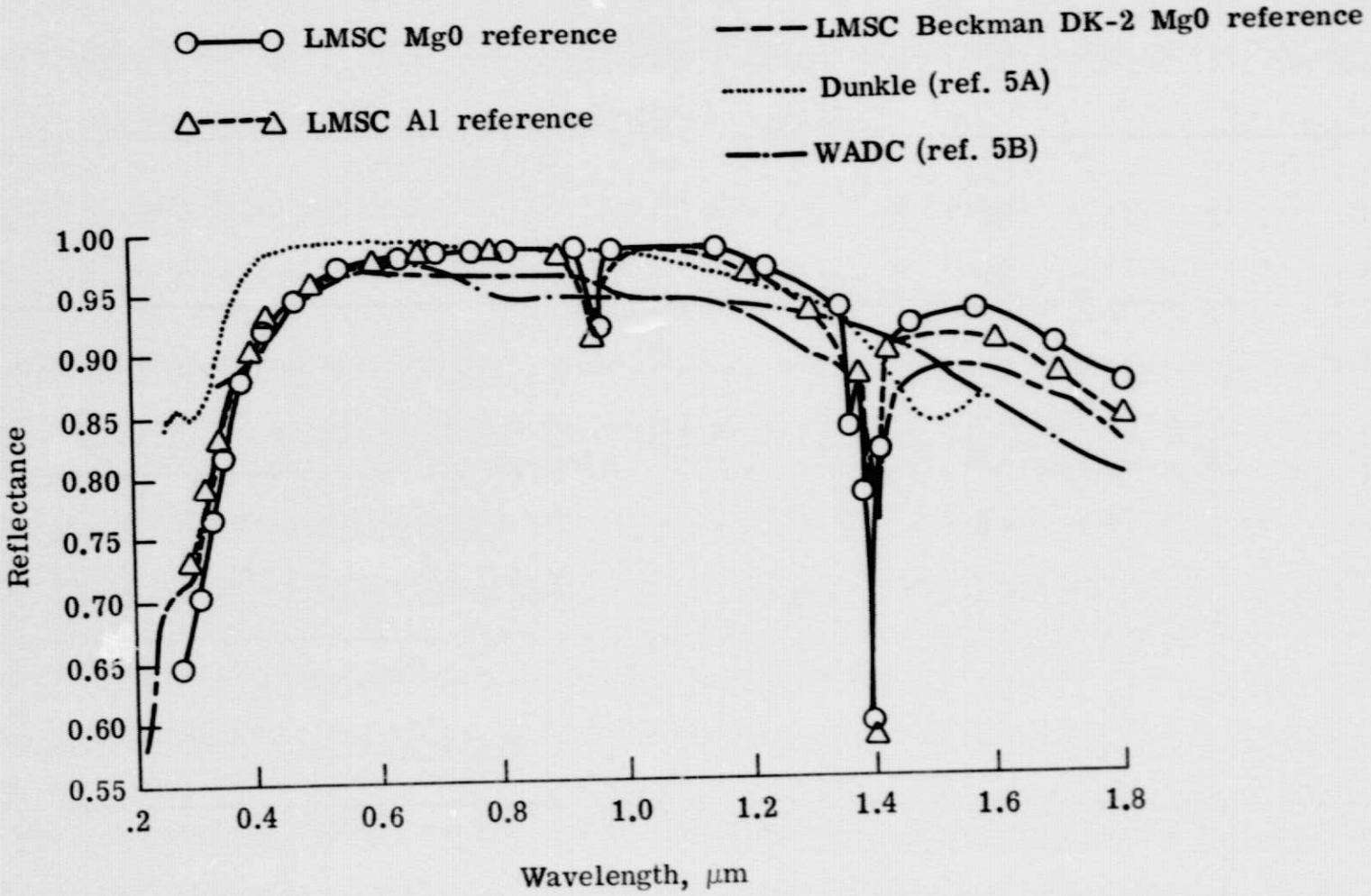


Figure 6.- The reflectance of magnesium carbonate (from reference 5).